IRAQI JOURNAL OF APPLIED PHYSICS
Vol. 19, No. 4B, November 2023, pp. 151-156

Heba H. Ali
Mazin A. Alalousi

Department of Physics,
College of Science,
University of Anbar,
Ramadi, IRAQ

Initial Characterization of the Prepared Au-Decorated TiO_2:Fullerene Films Using Electrospray Method

This study aims to enhance the properties of fullerene composite films and investigate the impact of incorporating TiO_2 on their structural, topographic, and optical characteristics. A hybrid method was employed to prepare these composite films by combining laser ablation to produce the colloidal of carbon, titanium dioxide and gold, then using the electro-spraying technique to produce TiO_2:fullerene films and then decorate them with gold nanoparticles. Addition of TiO_2 and decoration by gold have led to variations in the structural phases and a decrease in both crystallite and particle sizes. Similar effects were observed for band gap energy and Urbach energy.

Keyword: Titanium dioxide; Fullerene; Electro-spray; Wasted batteries; Laser ablation
Received: 31 July 2023; **Revised:** 28 August 2023; **Accepted:** 04 September 2023

1. Introduction

Carbon-based nanomaterials, such as graphene, fullerenes, carbon nanotubes, and carbon dots, have been extensively studied [1]. One of fullerenes is C_{60} also known as buckminsterfullerene or simply fullerene, is a carbon-based nanomaterial with consisting of 60 carbon atoms arranged in a hollow sphere [2]. Due to its unique a unique structural, electronic, and optical properties [3], involves many applications including photo-optical, supercapacitors, biomedical [4], drug delivery [1] applications. Addition to transistors and solar cells [5]. Titanium oxide (TiO_2) in one-dimensional (1D) nanostructure has a large surface/volume, a volume of the pore, and a mean-free-path length of electrons comparable with the two directions perpendicular to the long axis of the particles [5-9]. Therefore, TiO_2 with these properties is attractive and promising to the high-activity TiO_2-based photocatalyst [10-13]. Despite the relatively large gap in TiO_2 (more than a volt), the presence of C_{60} provides a smooth transfer of electrons in the presence of ultraviolet radiation, as it is in the presence of the non-local P structure that acts as a good acceptor for photocatalyzed electrons. In the C_{60}/TiO_2 system, the conduction band of TiO_2 is higher compared to that of $C_{60}/C_{60}^{\cdot-}$ (vs. NHE), so photoelectrons can transfer from TiO_2 nanoparticles to C_{60} in the presence of UV light [14]. Moreover, the amalgamation of TiO_2 and C_{60} results in heightened absorption attributed to an increase in surface electric charge. This, in combination with the heightened Schottky barrier between the deposited noble metal and the electron catalyst, serves to facilitate the capture of electrons by the noble metal. Consequently, it impedes the recombination of electron-hole pairs and amplifies the interaction for interfacial charge transfer. In this perspective, TiO_2 and gold decoration are expected to improve the optical properties of fullerenes towards photocatalysis [15]. Figure (1) explains the electronic reaction between C_{60} and TiO_2.

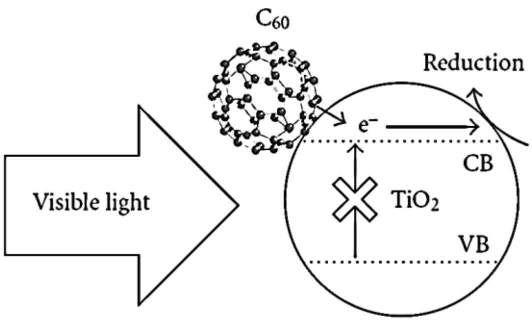

Fig. (1) A diagram of the photoelectron transfer model of TiO_2-C_{60} composite by visible light effect [18]

The photocatalytic activity enhancement of C_{60} and some compounds by C_{60} were discussed by many studies, such as Yu et al. [14], who have synthesized fullerene-modified TiO_2 nanocomposites and studied the enhancement of photocatalytic activity of the C_{60}/TiO_2 nanocomposites. Dai et al. [16] have improved the photocatalytic of the modifying $PbMoO_4$ by C_{60}. Tahir et al. [17] have fabricated fullerene-WO_3 composite systems for the photocatalytic. Also, Shahzad et al. [18] have fabricated heterojunction composites from WO_3/fullerene/Ni_3B/$Ni(OH)_2$ structures. Peng [19] has reported a theoretical study on the ability of using a Monolayer Fullerene Networks (MLFN) as photocatalyst for water treatment. In 2022, Fadhil et al. have studied the photocatalytic behaviour of C_{60}-TiO_2-ZnO, C_{60}-ZnO, C_{60}-TiO_2 nanocomposites. Liping et al. [20] have enhanced it by creating C_{60}@NU-901. Likewise, Munawar et al. [21] have fabricated a dual-functional La_2O_3–C_{60}

nanocomposite as an effective photocatalyst and supercapacitors electrode.

In this study, the structural, morphological, and optical properties, of Au-decorated TiO_2:fullerene films were investigated as a proposed photocatalyst.

2. Materials and Method

Carbon pellet extracted from battery electrodes were prepared by pressing carbon powders by means of a hydraulic press [22]. The same applies to TiO_2 powder to fabricate a TiO_2 pellet, which was placed in 50 ml of deionized water (DW), then bombarded with 3000 shots from pulsed Nd:YAG laser of 1064 nm wavelength and 100 mJ energy. The duration, width, and intensity of laser at the spot of shot were 6 Hz, 10 nm, and 4 $J.cm^{-2}$, respectively, and the distance between the surface target and the laser source was 12 cm. Then, carbon/TiO_2 colloidal was prepared by irradiating the carbon pellet in colloidal TiO_2 in 10, 30, and 50 vol.% of 50 ml of DW using the same laser parameters as well as the same number of laser shots. Finally, for decoration, the prepared films were sprayed by gold nanoparticles (AuNPs) colloidal, which was prepared with the same previous condition, but 1000 laser shots.

Carbon colloidal of 50 ml was sprayed on quartz and Au-coated glass substrates at 300±25 °C by electrospray technique with dc electrical bias potential of 5 kV, flow rate about 1 ml/min, ON/OFF spraying time of 10 and 30s, respectively. Figure (2) shows the schematic of the electrospray device used in this work.

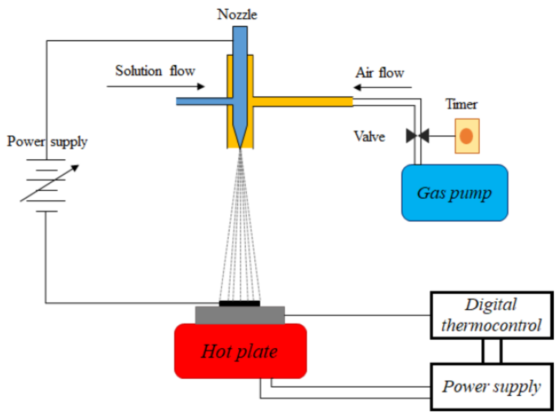

Fig. (2) Schematic of the electrospray device used in this work

The structural properties of the prepared films were performed on x-ray diffractometer (XRD) using CuKα radiation and accelerated voltage of 40 kV. The crystallite size had been estimated based on the Williamson-Hall relation [23]

$$D_{hkl} = \left(\frac{A\lambda}{cos\theta.\beta_{hkl}}\right) + (4\varepsilon \sin\theta) \qquad (1)$$

where D (nm) is the crystallite size, A is a dimensionless shape factor (0.89), λ is the wavelength of the x-ray beam (nm), β_{hkl} is the full-width at half maximum (FWHM) of the diffraction peaks, ε is the strain, and θ (rad) is the diffraction angle

The quantitate phase measurements were achieved using the reference intensity ratio (RIR) method [22]. A field-emission scanning electron microscope (FE-SEM, INSPECT-550) was used to introduce the surface morphology of the prepared films. The optical properties of the prepared films were investigated using a PG-T-80 UV-Visible spectrophotometer in the spectral range 200-900 nm.

3. Result and Discussion

The XRD patterns of the prepared films have been analyzed based on ICSD 98-060-2518, ICSD 98-005-6668, ICSD 98-009-5370, ICSD 98-007-5506, ICSD 98-000-9161, ICDD 98-005-6902, and ICSD 98-005-6909 cards for C_{60}, C_{60}–Polymeric, C_{70}, TiO_2 (Rutile), $C_{14}H_{10}$ (Ravatite), and $C_{20}H_{36}$ (Dinite). The thumbnail at the top of Fig. (3) represents the real XRD pattern of pure fullerene, in which the amorphous phase is hidden. Figure (3) shows XRD patterns of the prepared fullerenes films. XRD pattern of the prepared carbon films appears to be polycrystalline of C_{60} in (211), (311), (146), (352), and (651), where the dominant phase was (311) at 20.77° with crystallite size of about 80.76 nm, in conjunction with two structures: C_{60}-polymer (333), (170), and (600), and both (420) and (307) for C_{70}. It is clear that the addition of TiO_2 has led to significant changes in the structures, as shown in diffraction patterns. There is instability in the dominant phase site with variation of TiO_2 ratio and structures with the adding of TiO_2 [24]. At TiO_2 of 10 vol.%, the C_{60}-polymer ratio increased significantly with emergence of $C_{14}H_{10}$ phase (102). This structure is possibly a result of the dissociation of one of the fullerene molecules because of the high temperature and pressure in the plasma bubble generated by the laser in the presence of hydrogen resulting from the instantaneous dissociation of water with the same reason. The dominant phase is (600) which related to C_{70} with crystallite size of about 69 nm with a decrease in the quantity ratio to C_{60} as shown in table (1). With TiO_2 of 30 vol.%, it was observed that the polymerization continued to dominate the structure and the dominating phase returned to C_{60} (221) at 20.81° with crystallite size of about 31.68 nm and an increase of both RIR of C_{60}–Polymeric and C_{70} and vanishing of $C_{14}H_{10}$ phase. It is interesting that when the percentage of TiO_2 was increased to 50 vol.%, a phase emersion of Bis(cyclopentadienyl)bis(m-methoxybenzoato) titanium(IV) $Ti_4C_{104}O_{24}$ was observed. This result confirms the reaction of the Ti^+ ion with carbon atoms and O^- ion. The dominate phase was related C_{70} (141) at 21.60° in conjunction a drastic drop in RIR and an increase for C_{60} and C_{70}, respectively. Moreover, no peaks were seen for AuNPs due to their small amount.

 ISSN (print) 1813-2065, (online) 2309-1673

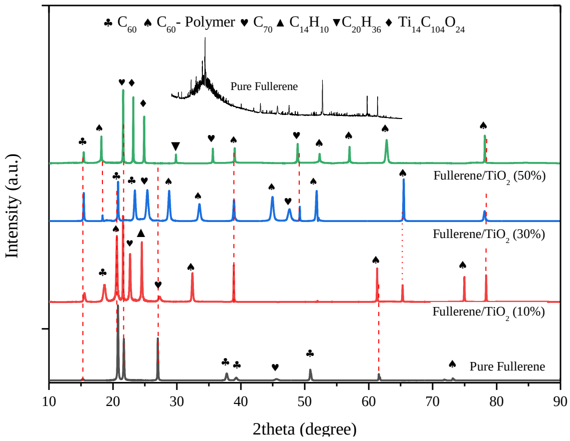

Fig. (3) XRD patterns of the prepared fullerenes and Au-decorated TiO_2:fullerene films

Table (1) Influence of TiO_2 addition on the RIR of the prepared Au-decorated TiO_2: fullerene films

Ratio of TiO_2 (vol.%)	C_{60} (%)	C_{60}–Polymeric (%)	C_{70} (%)
0	48.4700	5.51	46.02
10	6.7400	22.42	35.54
30	13.8800	70.64	15.48
50	2.9315	31.68	30.32

Figure (4) represents images of the prepared fullerenes and Au-decorated TiO_2:fullerene films. Fullerene films showed a variety of different shapes of nanoparticles, it is remarkable that there is a type of separation between the different particles, especially the rods. These nanorods can be C_{60}-polymeric with an average diameter of 39 nm, as shown in Fig. (4a). The separation between the particles and the inhomogeneity of the distribution can be attributed to the segregation of impurity phenomena as a result of the difference in the surface energy of the different particles [25]. Figure (4b) shows a better distinction for polymeric C_{60} with a change in the form of the formed particles that appear like disks longitudinally stacked (about 80 nm of thickness) tablets interspersed with spherical particles (about 34 nm of size) as they approach the assembly line. Increasing of TiO_2 ratio to 30 and 50 vol.% has led to appearance of material as heterogeneous aggregates with undifferentiated components as shown in figures (4c) and (4d). For clarity, the thumbnail images have been processed at a lower magnification to show the general distribution pattern of the deposited films. It appears that there is an evolution of the texture, where becomes more regular (as a fiber structure) with increasing TiO_2 ratio and begins to lose its agglomerated state in the form of fibrils when increasing to 50 vol.%. The cross section images of films showed a change in the deposited thickness of films to be 1172±664, 1373±217, 579±238.8, and 540±199.8 nm for 0, 10, 30, and 50 vol.% of TiO_2 ratio, respectively, as shown in Fig. (4e, f, g, and h).

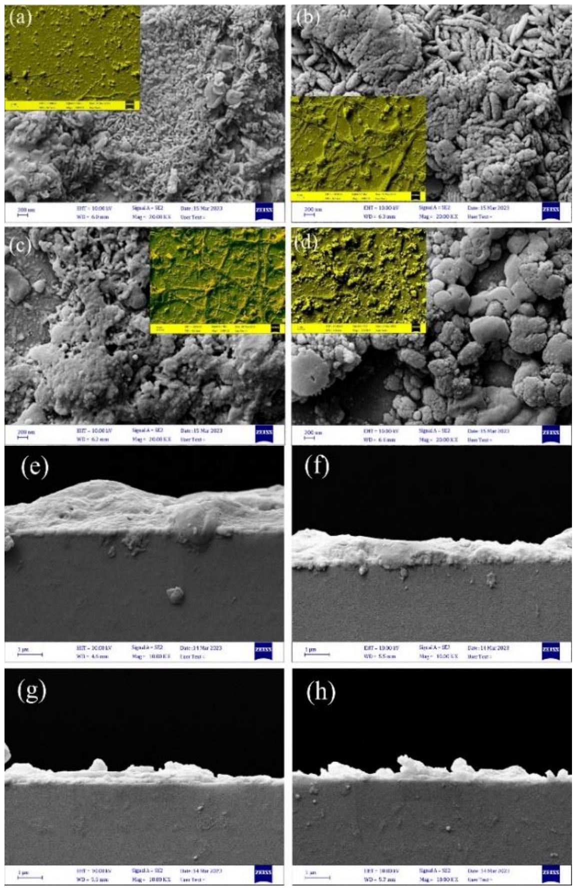

Fig. (4) FE-SEM images of the prepared Au-decorated TiO_2:fullerene films (a, b, c, and d) for the surface, (e, f, g, and h) for thickness

Figure (5) illustrates the behavior of the optical absorption of the prepared films. Fullerene displays a very interesting, complex and characteristic absorption spectrum with UV light because it has 30 weakly conjugated double bonds. Fullerene shows two intense bands at about 210 and 275 nm. The other absorption band of fullerene appearing in the UV region is located at about 330 nm. In the visible region, the spectrum of fullerene is dominated by a band at about 404 nm and by a broad and relatively weak groups of band between 430 and 670 nm with subfeatures at 500, 530, 570, 600, and 628 nm [26-29]. Clearly, at 210 nm, there is relatively high absorption with decreasing and shift by adding of TiO_2, blue shift for 30 and 50 vol.% and red for 10 vol.%, while at 385 nm for 0 vol.% TiO_2, which is related to a peak of 410 nm (as previous studies mentioned [9]), the spectrum suffered from a blue shift due to containing other structural phases as shown in the XRD pattern in Fig. (3). Concurrently, adding TiO_2 has led this peak to expand and merge with the previous one for both 10 and 50 vol.%, while its prominence is clear at 30 vol.%, which may be related to the increase of C_{60}-polymeric. There was also a clear decrease in the absorbance of films with a 30 vol.% TiO_2 ratio. The XRD pattern of fullerene:TiO_2 (30 vol.%) showed the absence of any structures outside the fullerene structures, which led to the abundance of TiO_2 without linkage that caused dominance of the optical TiO_2 behavior in addition to heavy attendance of C_{60}-polymeric [18]. Although the peaks of 500 and 530 nm (which is believed to be a contribution from the localized surface plasmon resonance (LRSP) of AuNPs) did not appear in the reference films as they became transparent when adding TiO_2 at all ratios with a clear convexity in the spectrum within the 550 nm regions down. This appearance can be confirmed as it represents the plasmon peak of AuNPs added as a decoration.

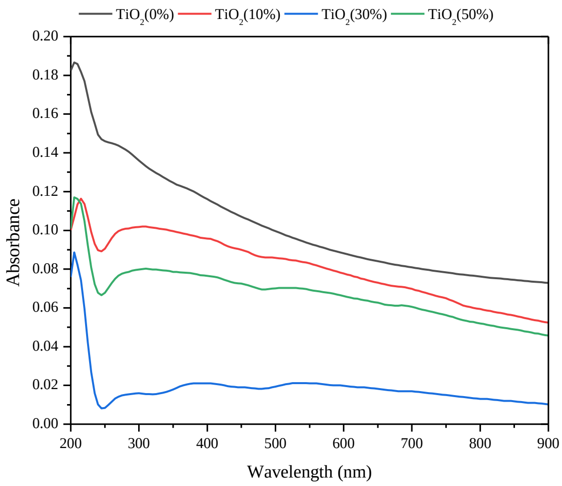

Fig. (5) Absorption spectra of the prepared Au-decorated TiO_2:fullerene films with different ratios of TiO_2

The bandgap energy (E_g) can be estimated by the Tauc's equation as [28]

$$\alpha h\upsilon = A(h\upsilon - Eg)^n \quad (2)$$

where $h\upsilon$ is the photon enery, α is the absorption coefficient, A is a constant, and n has the values of 1/2 and 2/3 for direct and indirect transitions, respectively

The plots of $(\alpha h\upsilon)^{1/2}$ versus $h\upsilon$ are depicted in Fig. (6) for all samples. Increasing TiO_2 ratio has clearly influenced the values of bandgap of the prepared Au-decorated TiO_2:fullerene films, as the bandgap was decreased with increasing TiO_2 ratio. Although, the energy gaps of C_{60} and C_{70} obtained from this study are large when compared to the typical values (1.86 and 1.57 eV). The lack of complete purity of the prepared films (containing amorphous phases) as proven by the analysis of the XRD patterns (Fig. 3), will lead to a large difference in the values of the energy gap and the mechanisms used by the material in the optoelectronic transitions, as exploded in table (2).

Table (2) Summary of influence of TiO_2 addition on the bandgap and Urbach energies of the prepared Au-decorated TiO_2:fullerene films

Ratio of TiO_2 (vol. %)	E_g (eV)	E_u (eV)	Crystallite Size (nm)	Lattice Strain [%]
0	2.15	3.60	80.74	0.265
10	1.87	1.36	69.02	0.298
30	1.63	1.42	31.68	0.213
50	1.62	1.42	96.69	1.845

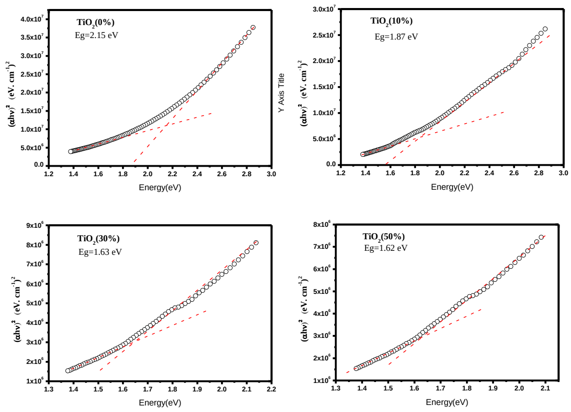

Fig. (6) The optical bandgap of the prepared Au-decorated TiO_2:fullerene films with different TiO_2 ratios

Urbach energy (E_u) related to both band tails of the localized states with the microstructural lattice disorders, and the crystal defects, can be estimated by the follwoing [29]

$$\alpha = \alpha_o exp\left(\frac{h\upsilon}{E_u}\right) \quad (3)$$

Figure (7) is a graphical representation of Eq. (3) for the prepared films with varying TiO_2 ratio, where E_u or the disturbance can be estimated by calculating the reverse slope of the linearly fitted line. However, E_u decreases with increasing TiO_2 ratio but keeps constant with 30 and 50 vol.%. Smaller strain decreases the structural disorder since it will influence the built-in electric field at the grain boundary and hence will consequently inhibit a disturbance of the density of the states [29,30]. Referring to the calculations derived from the analysis of the XRD patterns, it is noted that there is a correlation between the values of the Urbach energy and the strain values for the ratios of 0, 10, and 30 vol.%.

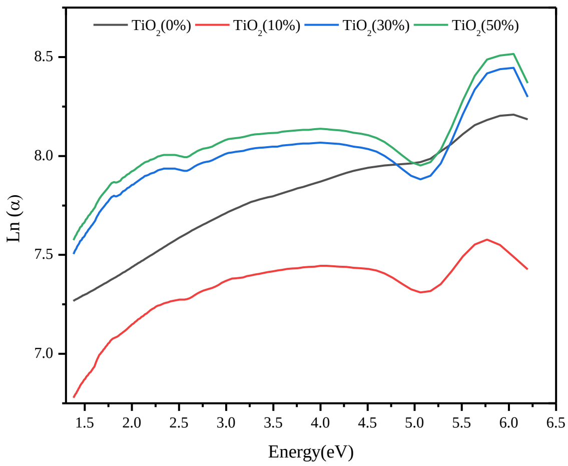

Fig. (7) Urbach energies of the prepared Au-decorated TiO_2:fullerene films as functions of energy

4. Conclusion

Au-decorated TiO_2:fullerene films were successfully prepared to produce fullerene and TiO_2:fullerene composites. The wasted batteries

 ISSN (print) 1813-2065, (online) 2309-1673

were used as a source for the pure carbon. In general, structural, morphological, and optical properties were affected by the variations in TiO_2 ratio in the prepared composites mainly on the crystalline phases, surface formation, and optical properties. These results encourage the selection of dry battery electrodes as a raw source for fullerenes and the Au-decorated TiO_2:fullerene films in several applications, such as photodetectors, gaseous and biosensors based on photocatalytic activity of such films.

References

[1] E. Özkan et al., "Sensor application of doped C_{60} fullerenes in detection of 1-(3-trifluoromethylphenyl)piperazine as an alternative to ecstasy", *Main Gr. Met. Chem.*, 42 (2019) 23-27.

[2] D.A. Heredia et al., "Fullerene C_{60} derivatives as antimicrobial photodynamic agents", *J. Photochem. Photobiol. C Photochem. Rev.*, 51 (2022) 100471.

[3] C. Ji et al., "Recent Developments of Carbon Dots in Biosensing: A Review", *ACS Sensors*, 5 (2020) 2724-2741.

[4] Y.Z.C. Ji, R.M. Leblanc and Z. Peng, "Recent Developments of Carbon Dots in Biosensing: A Review", *ACS Sensors*, 5 (2020) 2724-2741.

[5] S.H. Faisal and M.A. Hameed, "Heterojunction Solar Cell Based on Highly-Pure Nanopowders Prepared by DC Reactive Magnetron Sputtering", *Iraqi J. Appl. Phys.*, 16(3) (2020) 27-32.

[6] R.H. Turki and M.A. Hameed, "Spectral and Electrical Characteristics of Nanostructured NiO/TiO_2 Heterojunction Fabricated by DC Reactive Magnetron Sputtering", *Iraqi J. Appl. Phys.*, 16(3) (2020) 39-42.

[7] M.A. Hameed, S.H. Faisal, R.H. Turki, "Characterization of Multilayer Highly-Pure Metal Oxide Structures Prepared by DC Reactive Magnetron Sputtering Technique", *Iraqi J. Appl. Phys.*, 16(4) (2020) 25-30

[8] O.A. Hammadi, "Effects of Extraction Parameters on Particle Size of Titanium Dioxide Nanopowders Prepared by Physical Vapor Deposition Technique", *Plasmonics*, 15 (2020).

[9] F.J. Al-Maliki et al., "Enhanced photocatalytic activity of Ag-doped TiO_2 nanoparticles synthesized by DC Reactive Magnetron Co-Sputtering Technique", *Opt. Quantum Electron.*, 52 (2020) 188.

[10] E.A. Al-Oubidy and F.J. Al-Maliki, "Effect of Gas Mixing Ratio on Energy Band Gap of Mixed-Phase Titanium Dioxide Nanostructures Prepared by Reactive Magnetron Sputtering Technique", *Iraqi J. Appl. Phys.*, 14(4) (2018) 19-23.

[11] F.J. Al-Maliki and E.A. Al-Oubidy, "Effect of gas mixing ratio on structural characteristics of titanium dioxide nanostructures synthesized by DC reactive magnetron sputtering", *Physica B: Cond. Matter*, 555 (2019) 18-20

[12] O.A. Hammadi, F.J. Kadhim and E.A. Al-Oubidy, "Photocatalytic Activity of Nitrogen-Doped Titanium Dioxide Nanostructures Synthesized by DC Reactive Magnetron Sputtering Technique", *Nonl. Opt. Quantum Opt.*, 51(1-2) (2019) 67-78.

[13] E.A. Al-Oubidy and F.J. Al-Maliki, "Photocatalytic activity of anatase titanium dioxide nanostructures prepared by reactive magnetron sputtering technique", *Opt. Quantum Electron.*, 51(1-2) (2019) 23.

[14] D. Thakur et al., "Self-stability of un-encapsulated polycrystalline $MAPbI_3$ solar cells via the formation of chemical bonds between C60 molecules and MA cations", *Sol. Ener. Mater. Sol. Cells*, 235 (2022) 111454.

[15] J. Yu et al., "Enhanced photocatalytic activity of bimodal mesoporous titania powders by C_{60} modification", *Dalt. Trans.*, 40 (2011) 6635-44.

[16] Y.Z. Long et al., "Effect of C_{60} on the photocatalytic activity of TiO_2 nanorods", *J. Phys. Chem. C*, 113 (2009) 13899-13905.

[17] K. Dai et al., "Enhancing the photocatalytic activity of lead molybdate by modifying with fullerene", *J. Mol. Catal. A Chem.*, 374-375 (2013) 111-117.

[18] M.B. Tahir et al., "Role of fullerene to improve the WO_3 performance for photocatalytic applications and hydrogen evolution", *Int. J. Energy Res.*, 42 (2018) 4783-4789.

[19] K. Shahzad, M.B. Tahir and M. Sagir, "Engineering the performance of heterogeneous WO_3/fullerene@Ni_3B/$Ni(OH)_2$ Photocatalysts for Hydrogen Generation", *Int. J. Hydrog. Ener.*, 44 (2019) 21738-21745.

[20] B. Peng, "Monolayer Fullerene Networks as Photocatalysts for Overall Water Splitting", *J. Am. Chem. Soc.*, 144 (2022) 19921-19931.

[21] L. Liu et al., Enhancing Built-in Electric Fields for Efficient Photocatalytic Hydrogen Evolution by Encapsulating C_{60} Fullerene into Zirconium- Based Metal-Organic Frameworks, *Angew. Chemie.*, 135 (2023) e202217897.

[22] T. Munawar et al., "Fabrication of fullerene-supported La_2O_3–C_{60} nanocomposites: dual-functional materials for photocatalysis and supercapacitor electrodes", *Phys. Chem. Chem. Phys.*, 25 (2023) 7010-7027.

[23] B.M.A. Alani and M.A. Alalousi, "Structural, Morphological, and Spectroscopical Properties of Fullerenes (C_{60}) Thin Film Prepared via Electrospray Deposition", *IOP J. Phys.: Conf. Ser.*, 1829 (2021) 012018.

[24] F.J. Al-Maliki, O.A. Hammadi and E.A. Al-Oubidy, "Optimization of Rutile/Anatase Ratio in Titanium Dioxide Nanostructures prepared by DC Magnetron Sputtering Technique", *Iraqi*

J. Sci., 60(special issue) (2019) 91-98.

[25] S. Ilyas et al., "X-ray diffraction analysis of nanocomposite Fe_3O_4/activated carbon by Williamson–Hall and size-strain plot methods", *Nano-Struct. Nano-Obj.*, 20 (2019) 100396.

[26] M.A. Alalousi et al., "Sensing Enhancement of Gold Nanoparticles Doped-TiO_2 Thin Films as H_2S Gas Sensor", *Nano Hybrids Compos.*, 35 (2022) 1-10.

[27] F. Cataldo, S. Iglesias-Groth and A. Manchado, "On the molar extinction coefficient and integrated molar absorptivity of the infrared absorption spectra of C_{60} and C_{70} fullerenes", *Fuller. Nanotubes Carbon Nanostruct.*, 20 (2012) 191-199.

[28] K.I. Katsumata, N. Matsushita and K. Okada, "Preparation of TiO_2-fullerene composites and their photocatalytic activity under visible light", *Int. J. Photoener.*, 2012 (2012) 9.

[29] D. Patil et al., "Facile synthesis of stable Cu and CuO particles for 4-nitrophenol reduction, methylene blue photodegradation and antibacterial activity", *J. Hazard. Mater. Adv.*, 4 (2021) 100032.

[30] P. Norouzzadeh et al., "Investigation of structural, morphological and optical characteristics of Mn substituted Al-doped ZnO NPs: A Urbach energy and Kramers-Kronig study", *Optik*, 204 (2020) 164227.

 ISSN (print) 1813-2065, (online) 2309-1673